CARBON 94 (2015) 417–423

Contents lists available at ScienceDirect

CARBON

journal homepage: www.elsevier.com/locate/carbon

Carbon black/octadecane composites for room temperature electrical and thermal regulation

Yulong Wu, Xiaolu Yan, Peng Meng, Pengcheng Sun, Guoan Cheng, Ruiting Zheng *

Key Laboratory of Radiation Beam Technology and Materials Modification of Ministry of Education, College of Nuclear Science and Technology, Beijing Normal University, Beijing 100875, PR China

ARTICLE INFO

Article history:
Received 1 June 2015
Accepted 17 June 2015
Available online 25 June 2015

ABSTRACT

Electrical and thermal switchable materials are of interest in temperature regulation, circuit protection, sensors and other field. In this paper, functionalized carbon black (CB)/octadecane composites were synthesized for room temperature electrical and thermal switch. With these composites, large contrast ratios of electrical conductivity (EC) and thermal conductivity (TC) are achieved around the phase transition temperature (28–29 °C). The corresponding contrast ratios of EC and TC reach 4.3×10^5 and 3.3 times, respectively. The composites show remarkable stability and durability during the cycling experiments. The mechanisms of good stability and high EC contrast ratio are discussed as well.

1. Introduction

The materials for electrical regulation, i.e., thermistors attracted a lot of researchers' interest because of their potential applications in sensor, temperature control, thermal energy storage and other fields. Many kinds of thermistors, such as metal oxide [1–4], chalcogenides [5], ferroelectric ceramics [6–8] and polymer composites [9–12] have been developed in the past few decades. However, the transition temperatures of these thermistors do not lie in room temperature region. For example, the metal–insulator transition temperature of VO_2 is 340 K (67 °C), while the transition temperature of V_4O_7 is 250 K (−23 °C) [2]. It is a long standing demand to develop a kind of thermistor that works near the room temperature for the purpose of energy-saving and self-control.

The mechanisms of metal–insulator transition in oxide thermistors are based on solid-state phase transitions [1]. It's hard to adjust the transition temperature of these materials to room temperature. In the previous research, Zheng et al. [13] found that room temperature regulating of electrical and thermal conductivity can be realized via the solid–liquid transition in composites. Sun et al. [14] reported that the contrast ratio of electrical conductivity could be boosted to 5 orders of magnitude in the multi-walled carbon nanotube (MWCNT)/hexadecane composites by the surface modification of MWCNTs. In addition, Schiffres et al. [15] found that electrical and thermal conductivity contrast ratios of graphene/hexadecane composites can be tuned by changing freezing rates. The carbon nanomaterials and metal nanomaterials are good candidates for the additive of organic composite materials because of their excellent conductivity and good stability. For example, CNTs, graphite nanoplatelets, graphene oxide nanoparticles and graphene flakes are the applicable fillers in the polymer or grease composites. The thermal conductivity enhancement is above 100% for 1 wt% of the CNT or graphene loading [16–19]. The thermal conductivity of epoxy composite, 0.2 $W m^{-1} K^{-1}$ for the epoxy matrix, could be elevated to 5 $W m^{-1} K^{-1}$ by the volume fraction of 10% in graphene-multilayer graphene nanocomposites [17]. By choosing the appropriate matrix and additive, more electrical and thermal switch composites with different switch temperature can be designed for different applications.

In this paper, we report the functionalized carbon black/octadecane composites with high electrical conductivity (EC) and thermal conductivity (TC) contrast ratios, good stability and long-term durability. The phase transition temperature of octadecane is about 28 °C, which is an ideal matrix for the novel temperature switching composite that used in automatic air conditioning. We use conductive carbon black (CB) as additive because CB not only has excellent electrical and thermal conductivity [20–26], but also is much cheaper than carbon nanotube or graphene, which could greatly reduce the cost of composites. Via hydroxylation and esterification, functionalized CB nanoparticles dispersed uniformly in octadecane, which makes EC and TC contrast ratios of functionalized carbon black/octadecane composites reaches 4.3×10^5 and 3.3 times around the 28 °C. To our best knowledge, it is the highest EC contrast for these kinds of composites. At the end of this paper, the

* Corresponding author.
E-mail address: rtzheng@bnu.edu.cn (R. Zheng).

http://dx.doi.org/10.1016/j.carbon.2015.06.037
0008-6223/

effects of various carbon fillers on the EC and TC contrast ratios are discussed by comparing the results among carbon black, CNT and graphite flake composites.

2. Experiment

2.1. Materials

Carbon black (Vulcan XC72R) was purchased from Cabot Corp, MA, USA. Octadecane ($C_{18}H_{38}$), methylene chloride (CH_2Cl_2), acetic acid (CH_3COOH), tetrabutyl ammonium bromide (TBABr) and oleic acid ($C_{18}H_{34}O_2$) with analytical grade were purchased from Sinopharm Chemical Reagent Co., Ltd., China. Potassium permanganate ($KMnO_4$) and n-hexane (C_6H_{14}) with analytical grade were purchased from Beijing Chemical Reagent Co., China. All materials were used as received without further purification.

2.2. Preparation of functionalized CB/octadecane composites

The CB particles were functionalized by the method reported by Kim et al. [27]. Typically, 3 g of CB particles was dispersed in 300 mL of CH_2Cl_2 in a flask by the help of an ultrasonic probe (750 W). At the same time, 25 g of TBABr was dissolved in 50 mL of deionized (DI) water, 3.75 g of $KMnO_4$ was dissolved in 50 mL of DI water and then 120 mL of acetic acid was added. These kinds of solutions were added into the CB suspensions in sequence, and stirred vigorously for 24 h. After washing and freeze-drying, hydroxyl group modified CB (CB-OH) were obtained. Next, 2 g of CB-OH, 400 mL of n-hexane, and 40 g of oleic acid (OA) were added into a flask and stirred vigorously for 24 h at 60 °C. Then the mixture was washed and re-dispersed in n-hexane and filtered in order to remove the excess OA. Finally, the functionalized CB (CB-OA) was obtained after 24 h vacuum drying at room temperature. The functionalized CB particles were mixed with different amount of octadecane and vigorously stirred for 2 h in 70 °C water bath to obtain the functionalized CB/octadecane composites.

2.3. Characterization

The morphologies of CB particles were observed by a transmission electron microscope (TF20 Tecnai G^2, FEI) at 200 kV. The surface characteristics of CB, CB-OH and CB-OA particles were confirmed by X-ray photoelectron spectroscopy (ESCALAB 250Xi, Thermofisher). The cluster structures of the CB particles in octadecane were observed by optical microscope (Axio Imager A2m, Carl Zeiss) with the help of a LED backlight and a hot plate.

2.4. Electrical and thermal conductivity measurements

The electrical and thermal conductivity measurements were carried out by the technique reported in the previous work [13,14]. Briefly, the electrical resistance of composite was measured by pouring the liquid state composites into the rectangular cell that has two copper plate electrodes on opposite sidewalls. The measured cell was put into a thermostatic bath (Thermo Scientific HAAKE) and the temperature was maintained in 10–40 °C. A thermocouple (E-type) was placed in the central of the measured cell. The EC of the composite is given by the equation $\sigma = 1/\rho = L/RA = k/R$, where R is the measured resistance, L is the distance between the two electrodes and A is the area of plate electrode and $k = L/A = 4.4\ cm^{-1}$ is the cell constant. The uncertainty of EC measurement is estimated about 1.4%.

The transient hot-wire system [28] was used to measure the TC. In this work, we used a platinum hot wire with a 3 μm electrically insulating coating. The length of platinum wire is 70 mm and the diameter of which is 25 μm. The platinum was fully immersed in the liquid state samples, then the wire was subjected to an 80 mA current pulse and the power-on time was 2 s for every pulse. The resulting temperature rise was determined as a function of time by monitoring changes in the electrical resistance of the wire. The thermal penetration length in the sample was about 200 μm. We determined the TC of each sample by analyzing the temporal temperature profile and solving the heat conduction equation. The transient hot-wire system is calibrated by pure water and ethylene glycol before the TC measurement. The uncertainty estimated below 2%.

3. Results and discussion

Fig. 1 shows the morphologies and X-ray photoelectron spectroscopy (XPS) analysis of carbon black particles. It can be observed from Fig. 1(a) that the average diameter of primary particles is about tens of nanometer and these particles attached to each other and form aggregates with the size of several hundred nanometers to several micrometers. Fig. 1(b) is the HRTEM image of a typical CB particle. It shows that the primary CB particle is composed of short and defect carbon layers, the carbon layers arrange a round amorphous core and form an 'onion-like' microstructure, as reported by Pawlyta et al. [29]. The excellent EC and TC of CB particles originate from the stack of these carbon layers.

Chemical functionalization was applied to improve compatibility between CB particles and organic matrix. It has been proved to be a more effective method than the physical absorption of surfactants [27]. The surface structure of CB particles was characterized by XPS, as shown in Fig. 1(c)–(e). Fig. 1(c) shows the C1s spectrum of untreated CB, the peak at 284.4 eV is confirmed as C–C bonds. The insert photo in Fig. 1(c) indicates that untreated CB particles are hydrophobic and they are settled in organic matrix after 2 h of standing. After treated by $KMnO_4$ in acid environment, CB turns to be hydroxylated particles (CB-OH). In Fig. 1(d), the peaks at 285.5, 286.7 and 288.8 eV correspond to hydroxyl, epoxy or alkoxy, and carboxyl groups, respectively. These hydrophilic groups make CB-OH disperse well in water, but they are insoluble in organic matrix (insert photo in Fig. 1(d) shows the sample after 2 days of standing). When the oleic acid groups were further grafted on the surfaces of hydroxylated CB particles, the intensity of the XPS peak related to hydroxyl group was dramatically decreased, as shown in Fig. 1(e), and new peaks appeared at 287.5 and 288.3 eV. The new peaks should come from the carbonyl and ester groups after hydroxyl groups reacted with oleic acid [27,30]. The similar structures of the function groups and hexane make CB-OA hydrophobic again but disperse well in hexane after 2 days of standing, as insert photo in Fig. 1(e) shows. The steric effect of long-alkyl chain groups on the surface of CB particles makes particles repel each other and uniformly dispersed in nonpolar solvents.

After surface functionalization, CB-OA particles disperse uniformly in octadecane, and CB-OA/octadecane composites exhibit higher EC and TC contrast ratio. Fig. 2 shows EC and TC properties of CB-OA/octadecane composites with different volume fraction. From Fig. 2(a), it can be observed that the EC changes little with the variation of temperature at the liquid state (>30 °C) or solid state (<28 °C). However, it increases dramatically when the temperature decreases from 30 to 28 °C while there is little EC change in pure octadecane, which shows a negative temperature coefficient (NTC) behavior. It indicates that the composites transform from insulators to semiconductors. The EC contrast ratio, i.e., the ratio of EC in solid state to EC in liquid state, exceeds 4.3×10^5 at the volume fraction of 1.30%, corresponding EC of liquid and solid composites are 6.4×10^{-8} and $2.7 \times 10^{-2}\ S\ m^{-1}$, respectively. The similar tendency occurs in the TC of CB-OA/octadecane

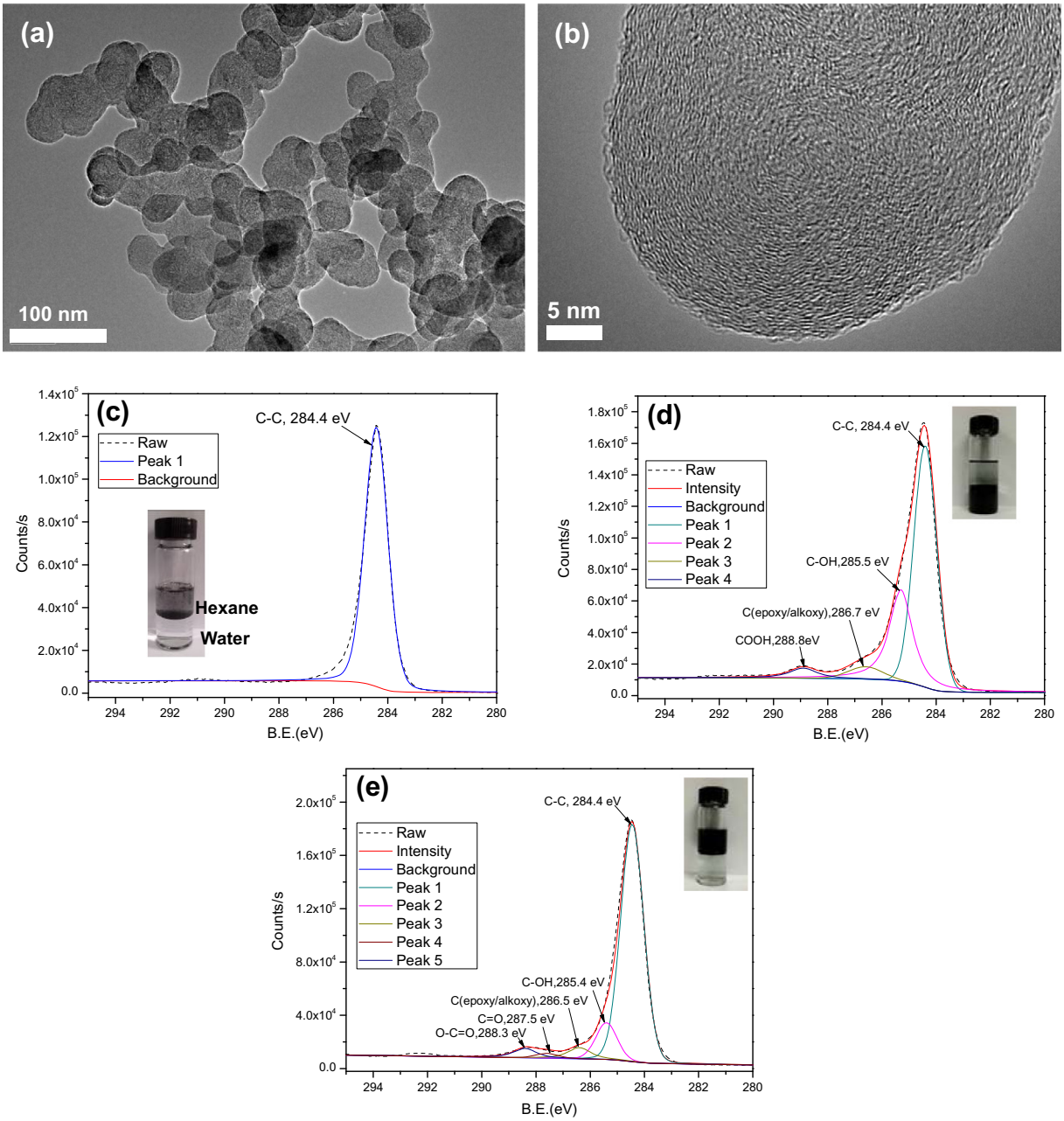

Fig. 1. The morphologies and XPS spectrums of carbon black. (a) TEM image of CB particles. (b) HRTEM image of a typical particle; (c)–(e) are the C1s XPS spectrums of CB, CB-OH, CB-OA, respectively. (The insert photos are the disperse states of the corresponding particles in different liquids, the top layer of liquid in the glass bottle is hexane and the bottom layer of liquid is water.)

composites (Fig. 2(b)). TC of the composites changes sharply during the phase transition, but it is stable in solid and liquid state. The biggest TC contrast ratio reaches 3.3 times at the volume fraction of 1.30% and the corresponding TC of liquid and solid composites are 0.158 and 0.525 W m^{-1} K^{-1}, respectively. The dramatic change of EC and TC around the phase transition temperature is caused by the variation of microstructure in the composites [13]. The network is loose and breakable in the liquid state due to the Brownian motion and convection effect. When the matrix freeze, the clusters will be squeezed to grain boundaries by the internal stress, and lead to a conductive percolation network in solid state, therefore the EC and TC would be promoted vastly.

The EC and TC of CB-OA/octadecane composites as a function of CB-OA volume fraction are shown in Fig. 2(c) and (d). The EC of composites at 34 °C (the liquid state) is about 6×10^{-8} S m^{-1}, varies little with the change of CB-OA volume fraction, as shown in Fig. 2(c). In the solid state, the corresponding EC increases from 6.8×10^{-8} S m^{-1} (0.43%) to the peak of 2.7×10^{-2} S m^{-1} (1.3%), then decreases slightly to 8.0×10^{-3} S m^{-1} at the volume fraction of 1.73%. It may be ascribed to the fact that partially agglomerated CB-OA particles would have a negative effect on the conductive paths at high concentration. The similar results were observed in other composites such as MWCNT/octadecane composites [31]. From Fig. 2(d), it can be observed that the variation of TC is similar to that of EC. In the liquid state, the TC of composites changes little, varies from 0.147 (0.43%) to 0.168 W m^{-1} K^{-1} (1.73%) with the increase of CB-OA loading. In the solid state, the corresponding EC increases from 0.368 W m^{-1} K^{-1} (0.43%) to the peak of 0.525 W m^{-1} K^{-1} (1.3%), then declining to 0.467 W m^{-1} K^{-1} (1.73%). The EC and TC contrast ratios as a function of CB-OA

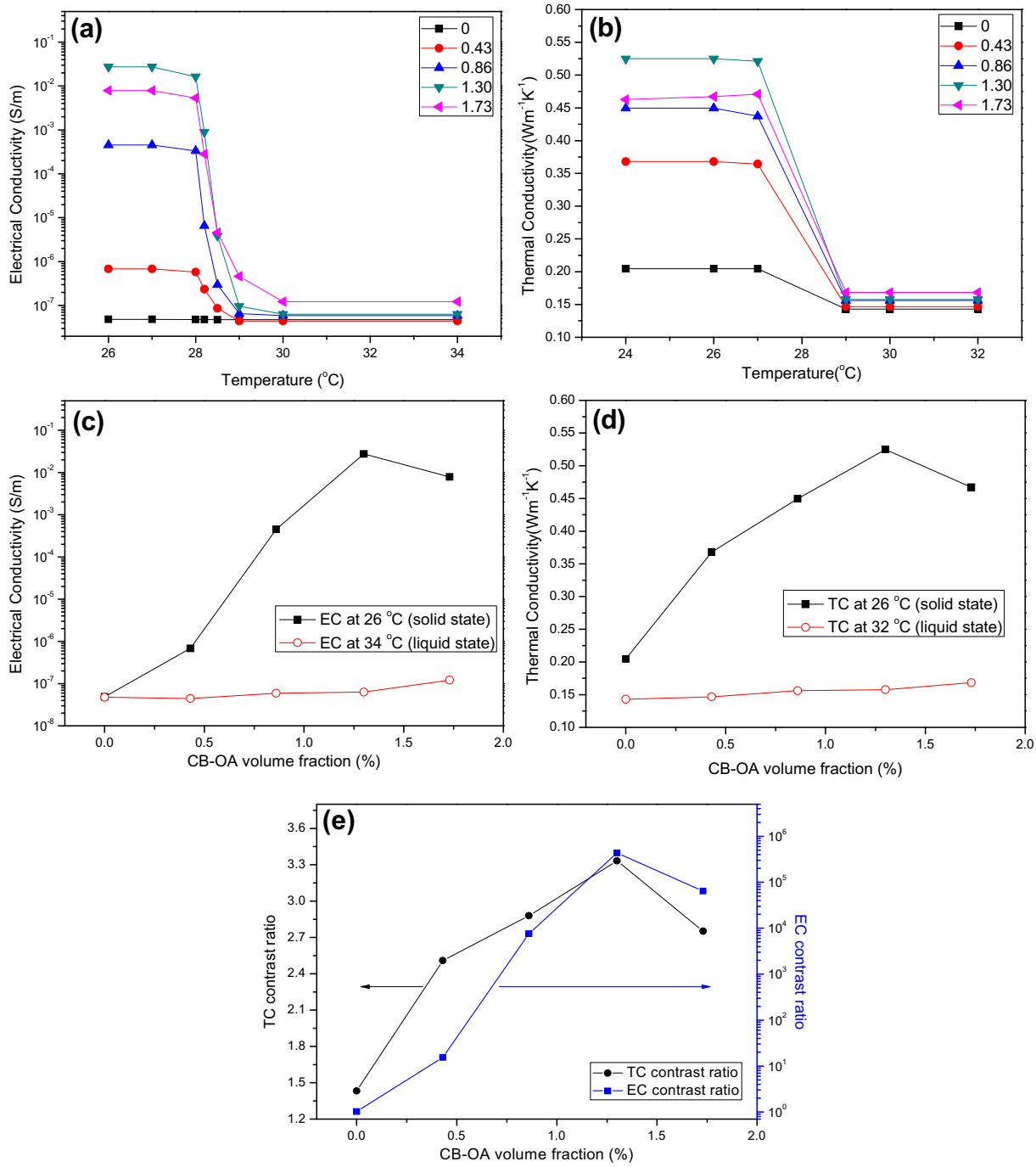

Fig. 2. EC and TC of CB-OA/octadecane composites around the phase transition point. (a) EC of composites near the room temperature, (b) TC of composites near the room temperature, (c) EC of composites as a function of CB-OA volume fractions, (d) TC of composites as a function CB-OA volume fractions, (e) contrast ratios as a function of CB-OA volume fraction.

volume fraction in composites are shown in Fig. 2(e). The EC and TC contrast ratios increase rapidly with the increase of CB-OA loading. It can be ascribed to the much more rapid increase of EC and TC in the solid state than that in the liquid state. The EC contrast ratios increase from 15 (0.43%) to the peak of 4.3×10^5 (1.3%) and the corresponding TC contrast ratios increase from 2.5 to 3.3 times. However, the contrast ratio decreases obviously when the CB-OA volume fraction exceeds 1.3%. The decrease of EC or TC in the solid state may account for the decrease of corresponding contrast ratio at high CB-OA loading.

The durability is important for the applications of the composite. We test the durability by temperature cycling experiments. Fig. 3(a) and (b) show the EC and TC cycling behavior of CB-OA/octadecane composites at the volume fraction of 1.3%. The EC contrast ratios increase in the first four cycles. It may be attributed to the slight growing up of CB-OA clusters, which makes the particles within clusters contact better. After 5 cycles, the EC contrast ratios become stable due to the stabilization of the CB-OA clusters after 5 times of phase transitions. Different from EC contrast, the TC contrast ratios change little during the cycles. It may be attributed to the different transport mechanism between electron and phonon. The bigger clusters would promote electron transport and would not necessarily increase phonon transport in composites [32–34]. Fig. 3(c) and (d) show the microstructure of

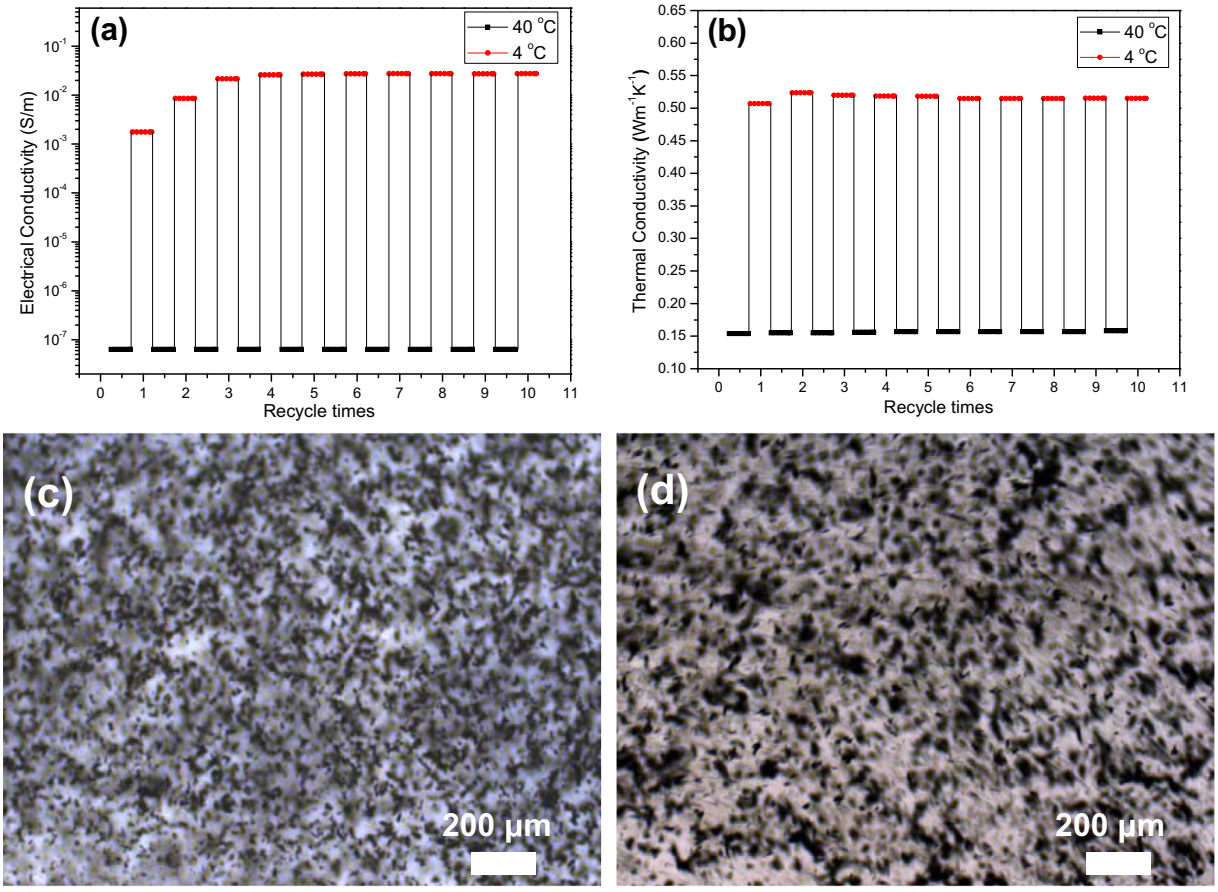

Fig. 3. (a) and (b) are EC and TC cycling behavior of 1.3 vol% CB-OA/octadecane composite, respectively. The EC and TC are measured at 4 and 40 °C. (c) and (d) are optical microscope images of CB-OA/octadecane composite with the volume fraction of 0.2%. (c) CB-OA clusters before the temperature cycle. (d) The CB-OA clusters after 10 temperature cycles.

CB-OA/octadecane composites with the volume fraction of 0.2%. Comparing with Fig. 3(c) and (d), we can found that the size of clusters is several to tens of micrometers and increases a little after 10 cycles, which indicates that the steric effect of long-alkyl chain groups is effective in preventing the small CB clusters to agglomerate during the phase transitions. The stable microstructure of CB-OA/octadecane composites results in the stable TC and EC contrast after ten cycles of freezing and remelting.

A direct comparison between the current results and the previous results [13,14] is shown in Fig. 4. It can be observed from Fig. 4(a) that the maximal EC contrast ratio of graphite/hexadecane composite is 250 at the volume fraction of 0.8%. The smaller EC contrast ratio of graphite/hexadecane composite can be attributed to the absence of surface functionalization and the large size of graphite nanoplatelets, which makes graphite composites have higher EC at liquid state. The maximum EC contrast of CB-OA/octadecane composite is 4.3×10^5 at the volume fraction of 1.3%, which is two times higher than that (1.6×10^5) of carbon nanotube composite. It is a new record among room temperature switch composites. Surface modification of CNT and CB not only improves the stability of composites but also enhances the contact resistance between particles, which will greatly increase the total contact resistance and decrease the EC in liquid composites. However, the particles are squeezed together in solid composites, the contact resistance decreases obviously. So the F-MWCNT and CB-OA composites show higher EC contrast. Round-sphere structure makes the total contact resistance of liquid CB-OA composites higher than that of liquid F-MWCNT composite, which is the reason that the highest EC contrast is observed in CB-OA composite. The EC contrast ratio peak is at the volume fractions of 0.8% in the graphite composites, but 1.2% and 1.3% in F-MWCNT composites and CB-OA composites, respectively. The difference should be attributed to the aspect ratios of particles [35–37]. The graphite nanoplatelets have an average diameter of several microns and a thickness from several nanometers to several tens of nanometers, the aspect ratio of which varies from several hundreds to 1000. The platelets can contact better and form more efficient conductive paths at lower volume fraction. The F-MWCNTs, with 0.5–2 μm in length and 15 nm in diameter, have the average aspect ratio of 100. The primary CB particles are quasi-spheral and the aspect ratio is close to 1, but the CB we used tend to aggregate and form a chain-like structure (Fig. 1(a)), the average aspect ratio would be closer to that of the nanotubes. Therefore, the volume fractions of EC contrast ratio peak in two types of composites are close.

The TC contrast ratios are shown in Fig. 4(b). The maximal TC contrast ratios of different nanocarbon composites are all above 3 times. The deviation is relatively small, but we still could get some clues about the effects of aspect ratio on the thermal properties. The volume fractions of TC contrast ratio peaks in three types of composites are 0.4% (FMWCNT), 0.8% (graphite) and 1.3% (CB-OA), respectively. Comparing with Fig. 4(a) and (b), we can find that both in the graphite and CB composites, the volume fraction of TC contrast ratio peak is consistent with that of EC contrast ratio peak. It is easy to understand because usually a good EC conductor is also a good TC conductor. However, the volume fractions of TC contrast ratio peak and EC contrast ratio peak are different in CNT composites. The reason is not well known at present. CNTs have excellent axial thermal conductivity and large aspect ratio.

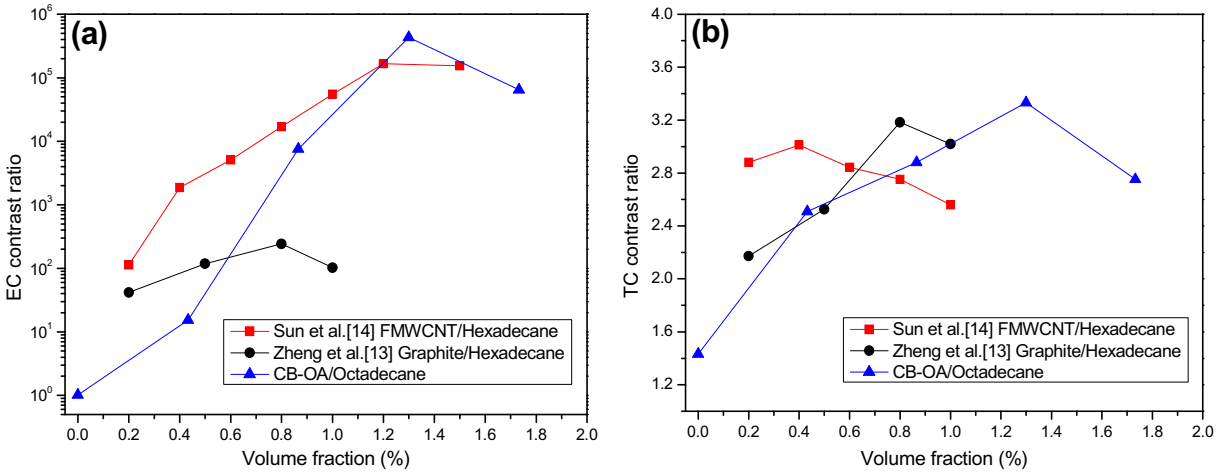

Fig. 4. The comparisons of the three types of composites. (a) EC contrast ratios, (b) TC contrast ratios.

However, the CNTs are easy to tangle in the composites. We conjecture that the cluster structure of CNT result in the different variation trend in TC contrast ratio, as other researchers also reported [38].

4. Conclusions

We reported a new kind of functionalized carbon black/octadecane switch materials for room temperature electrical and thermal regulation. The surface functionalization is proved to be an effective method to improve the durability and stability of the composites. The EC and TC of the composites show obvious switch properties around the phase transition temperature. The peaks of EC and TC contrast ratio are more than 5 orders of magnitude and 3.3 times at the volume fraction of 1.3%, respectively. The EC contrast ratio of CB-OA/octadecane is a new record among room temperature switch composites. The effects of carbon filler aspect ratios on the EC and TC contrast ratio are also be discussed at the end of paper. The low dimensional structure and surface functionalization of CB is the reason that CB-OA composite shows higher EC and TC contrast ratio and good stability. Because of their higher EC and TC contrast ratio and low cost, the functionalized carbon black/octadecane composites will have great application potential in the applications of overload protection, automatic temperature control and detection.

Acknowledgements

This work is supported by the Program for New Century Excellent Talents in University, Ministry of Education of China (NCET-11-0043) and the Fundamental Research Funds for the Central Universities of China.

References

[1] M. Imada, A. Fujimori, Y. Tokura, Metal–insulator transitions, Rev. Mod. Phys. 70 (4) (1998) 1039–1263.
[2] Z. Yang, C. Ko, S. Ramanathan, Oxide electronics utilizing ultrafast metal–insulator transitions, Annu. Rev. Mater. Res. 41 (2011) 337–367.
[3] T.W. Hickmott, Low-frequency negative resistance in thin anodic oxide films, J. Appl. Phys. 33 (9) (1962) 2669–2682.
[4] C. Wu, H. Wei, B. Ning, Y. Xie, New vanadium oxide nanostructures: controlled synthesis and their smart electrical switching properties, Adv. Mater. 22 (17) (2010) 1972–1976.
[5] D. Adler, Mechanisms for metal–nonmental transitions in transition-metal oxides and sulfides, Rev. Mod. Phys. 40 (4) (1968) 714–736.
[6] J.B. Torrance, P. Lacorre, A.I. Nazzal, E.J. Ansaldo, Ch. Niedermayer, Systematic study of insulator–metal transitions in perovskites $RNiO_3$ (R=Pr, Nd, Sm, Eu) due to closing of charge-transfer gap, Phys. Rev. B 45 (14) (1992) 8209–8212.
[7] R. Oligschlaeger, R. Waser, R. Meyer, S. Karthäuser, R. Dittmann, Resistive switching and data reliability of epitaxial (Ba, Sr) TiO_3 thin films, Appl. Phys. Lett. 88 (4) (2006) 042901–42903.
[8] K. Szot, W. Speier, G. Bihlmayer, R. Waser, Switching the electrical resistance of individual dislocations in single-crystalline $SrTiO_3$, Nat. Mater. 5 (4) (2006) 312–320.
[9] K. Ohe, Y. Naito, A new resistor having an anomalously large positive temperature coefficient, Jpn. J. Appl. Phys. 10 (1) (1971) 99–108.
[10] J. Meyer, Stability of polymer composites as positive-temperature-coefficient resistors, Polym. Eng. Sci. 14 (10) (1974) 706–716.
[11] M. Hindermann-Bischoff, F. Ehrburger-Dolle, Electrical conductivity of carbon black–polyethylene composites: experimental evidence of the change of cluster connectivity in the PTC effect, Carbon 39 (3) (2001) 375–382.
[12] Y. Xi, H. Ishikawa, Y. Bin, M. Matsuo, Positive temperature coefficient effect of LMWPE–UHMWPE blends filled with short carbon fibers, Carbon 42 (8) (2004) 1699–1706.
[13] R. Zheng, J. Gao, J. Wang, G. Chen, Reversible temperature regulation of electrical and thermal conductivity using liquid–solid phase transitions, Nat. Commun. 2 (2011) 289.
[14] P. Sun, Y. Wu, J. Gao, G. Cheng, G. Chen, R. Zheng, Room temperature electrical and thermal switching CNT/Hexadecane composites, Adv. Mater. 25 (35) (2013) 4938–4943.
[15] S.N. Schiffres, S. Harish, S. Maruyama, J. Shiomi, J.A. Malen, Tunable electrical and thermal transport in ice-templated multilayer graphene nanocomposites through freezing rate control, ACS Nano 7 (12) (2013) 11183–11189.
[16] A.A. Balandin, Thermal properties of graphene and nanostructured carbon materials, Nat. Mater. 10 (8) (2011) 569–581.
[17] K.M.F. Shahil, A.A. Balandin, Graphene-multilayer graphene nanocomposites as highly efficient thermal interface materials, Nano Lett. 12 (2) (2012) 861–867.
[18] R. Gulotty, M. Castellino, P. Jagdale, A. Tagliaferro, A.A. Balandin, Effects of functionalization on thermal properties of single-wall and multi-wall carbon nanotube–polymer nanocomposites, ACS Nano 7 (6) (2013) 5114–5121.
[19] J.D. Renteria, D.L. Nika, A.A. Balandin, Graphene thermal properties: applications in thermal management and energy storage, Appl. Sci. 4 (4) (2014) 525–547.
[20] M. Sumita, K. Sakata, S. Asai, K. Miyasaka, H. Nakagawa, Dispersion of fillers and the electrical conductivity of polymer blends filled with carbon black, Polym. Bull. 25 (2) (1991) 265–271.
[21] F. El-Tantawy, K. Kamada, H. Ohnabe, In situ network structure, electrical and thermal properties of conductive epoxy resin–carbon black composites for electrical heater applications, Mater. Lett. 56 (1) (2002) 112–126.
[22] S. Kang, A.R. Jones, J.S. Moore, S.R. White, N.R. Sottos, Microencapsulated carbon black suspensions for restoration of electrical conductivity, Adv. Funct. Mater. 24 (20) (2014) 2947–2956.
[23] M. Pelíšková, P. Piyamanocha, J. Prokeš, M. Varga, P. Sáha, The electrical conductivity of ethylene butyl-acrylate/carbon black composites: the effect of foaming on the percolation threshold, Synth. Met. 188 (2014) 140–145.
[24] C.K. Leong, D.D.L. Chung, Carbon black dispersions as thermal pastes that surpass solder in providing high thermal contact conductance, Carbon 41 (13) (2003) 2459–2469.
[25] D. Han, Z. Meng, D. Wu, C. Zhang, H. Zhu, Thermal properties of carbon black aqueous nanofluids for solar absorption, Nanoscale Res. Lett. 6 (1) (2011) 1–7.
[26] Z. Meng, D. Han, D. Wu, H. Zhu, Q. Li, Thermal conductivities, rheological behaviors and photothermal properties of ethylene glycol-based nanofluids containing carbon black nanoparticles, Proc. Eng. 36 (2012) 521–527.

[27] J.Y. Kim, J.Y. Oh, K.S. Suh, Voltage switchable surface-modified carbon black nanoparticles for dual-particle electrophoretic displays, Carbon 66 (2014) 361–368.
[28] Y. Nagasaka, A. Nagashima, Absolute measurement of the thermal conductivity of electrically conducting liquids by the transient hot-wire method, J. Phys. E: Sci. Instrum. 14 (12) (1981) 1435–1440.
[29] M. Pawlyta, J.N. Rouzaud, S. Duber, Raman microspectroscopy characterization of carbon blacks: Spectral analysis and structural information, Carbon 84 (2015) 479–490.
[30] H. Han, J. Lee, D.W. Park, S.E. Shim, Surface modification of carbon black by oleic acid for miniemulsion polymerization of styrene, Macromol. Res. 18 (5) (2010) 435–441.
[31] E.Ç. Bayramoglu, Thermal properties and stability of n-octadecane based composites containing multiwalled carbon nanotubes, Polym. Compos. 32 (6) (2011) 904–909.
[32] R. Prasher, P.E. Phelan, P. Bhattacharya, Effect of aggregation kinetics on the thermal conductivity of nanoscale colloidal solutions (nanofluid), Nano Lett. 6 (7) (2006) 1529–1534.
[33] J.E. Peters, D.V. Papavassiliou, B.P. Grady, Unique thermal conductivity behavior of single-walled carbon nanotube–polystyrene composites, Macromolecules 41 (20) (2008) 7274–7277.
[34] S.A. Angayarkanni, J. Philip, Role of adsorbing moieties on thermal conductivity and associated properties of nanofluids, J. Phys. Chem. C 117 (17) (2013) 9009–9019.
[35] B.X. Wang, L.P. Zhou, X.F. Peng, A fractal model for predicting the effective thermal conductivity of liquid with suspension of nanoparticles, Int. J. Heat Mass Transf. 46 (14) (2003) 2665–2672.
[36] P.E. Gharagozloo, K.E. Goodson, Aggregate fractal dimensions and thermal conduction in nanofluids, J. Appl. Phys. 108 (7) (2010) 074309.
[37] A.S. Cherkasova, J.W. Shan, Particle aspect-ratio and agglomeration-state effects on the effective thermal conductivity of aqueous suspensions of multiwalled carbon nanotubes, J. Heat Transfer 132 (8) (2010) 082402.
[38] J. Li, P.C. Ma, W.S. Chow, C.K. To, B.Z. Tang, J.K. Kim, Correlations between percolation threshold, dispersion state, and aspect ratio of carbon nanotubes, Adv. Funct. Mater. 17 (16) (2007) 3207–3215.